Determination of electronic band structures of $CaMnO_3$ and $LaMnO_3$ using optical-conductivity analyses

J. H. Jung,* K. H. Kim, D. J. Eom, and T. W. Noh†
Department of Physics, Seoul National University, Seoul 151-742, Korea

E. J. Choi
Department of Physics, Seoul City University, Seoul 130-743, Korea

Jaejun Yu
Department of Physics, Sojang University, Seoul 121-742, Korea

Y. S. Kwon
Department of Physics, Sung Kyun Kwan University, Suwon 440-746, Korea

Y. Chung
Pohang Accelerator Laboratory, POSTECH, Pohang 790-784, Korea
(Received 13 January 1997)

Reflectivity spectra of $CaMnO_3$ and $LaMnO_3$ were measured in a wide photon energy region between 5 meV and 30 eV at room temperature. Using the conductivity spectra obtained from the Kramers-Kronig analysis, electronic structures of the manganese oxides were investigated. In particular, the states near the Fermi energy E_F, O $2p$ and Mn $3d$ (e_g,t_{2g}), were studied in detail. It was found that the O $2p$ band is located closer to E_F than the Mn t_{2g} band. For $LaMnO_3$, the filled Mn $e_{g\uparrow}^1$ band is located closer to E_F than any other valence band. The t_{2g}-e_g Hund exchange energy was found to be about 3.4 eV and the Jahn-Teller stabilization energy E_0 was estimated to be less than 0.5 eV. [S0163-1829(97)04823-6]

Recently, a great deal of attention has been paid to the physical properties of the perovskite $La_{1-x}Ca_xMnO_3$ system due to its colossal magnetoresistance (CMR).[1] For doping levels with $0.2 \leqslant x \leqslant 0.5$, the system shows an insulator-metal transition accompanying a paramagnetic to ferromagnetic transition at T_c.[2]

To understand the intriguing properties of $La_{1-x}Ca_xMnO_3$, it is important to know electronic structures of the end members, i.e., $CaMnO_3$ and $LaMnO_3$. Electronic configurations of the Mn d electrons in $CaMnO_3$ and $LaMnO_3$ are t_{2g}^3 and $t_{2g}^3 e_g^1$, respectively. The energy separation between the e_g and the t_{2g} levels, caused by a crystal field splitting, is known to be larger than 1 eV.[3] For $LaMnO_3$, a static Jahn-Teller (JT) distortion lifts the degeneracy in the e_g level, splitting it into e_g^1 and e_g^2 levels.

In spite of intensive experimental[4–7] and theoretical[8–11] efforts to understand the electronic structures of the end members, there still exist some ambiguities on the valence-band structures. Both x-ray (XPS) and ultraviolet photoemission spectroscopy (UPS) experiments showed a double-peak structure between -10 eV and the Fermi energy E_F.[5–7] Even though it is widely accepted that the double-peak structure arises from O $2p$ and Mn d bands, an important controversy still remains: some have argued that the O $2p$ band lies below the Mn t_{2g} band,[8] while others have suggested the opposite.[9] The reported positions of the $e_{g\uparrow}^1$ band in $LaMnO_3$ are also different.[6,9] Moreover, x-ray absorption spectroscopy (XAS) data showed that several apparent peaks exist up to 5 eV above E_F, but some disputes still remain about the origins of those conduction-band peaks.[4–6]

In this paper, we report optical conductivity spectra of $CaMnO_3$ and $LaMnO_3$. Combining them with earlier results from numerous spectroscopic measurements, we could establish detailed electronic structures, especially near E_F. Based on these findings, we were also able to determine some physical quantities, i.e., the t_{2g}-e_g Hund exchange and the JT stabilization energies. (As far as we know, it is the first experimental effort to determine values of such important quantities.)

Polycrystalline samples of $CaMnO_3$ and $LaMnO_3$ were prepared by the standard solid-state reaction method. X-ray powder diffraction measurements showed that both samples were single phase with orthorhombic crystal structures. Electron-probe microanalysis showed that chemical compositions of the samples were close to the stoichiometric values within an experimental error of 2%. Details on the sample preparation were published in earlier papers.[12,13]

Just before the optical measurements, the samples were polished up to 1.0 μm using diamond pastes. Near normal incidence reflectivity spectra of $CaMnO_3$ and $LaMnO_3$ were measured at room temperature. A Fourier transform spectrophotometer was used between 5 meV and 0.8 eV, and a grating monochromator was used between 0.6 and 7.0 eV. Above 6.0 eV, we used the synchrotron radiation from the Normal Incidence Monochromator beam line at the Pohang Light Source (PLS). To take surface scattering effects into account, gold films were evaporated on the polished samples just after the spectra were taken. Then, reflectivities of the gold-coated surfaces were measured again and used for substracting the scattering effects.

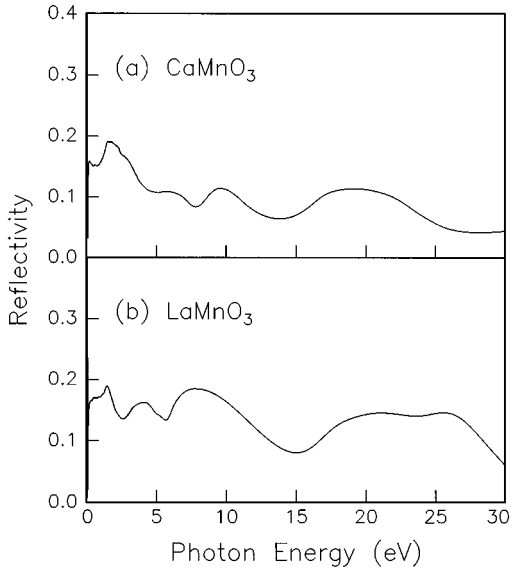

FIG. 1. Reflectivity spectra of (a) $CaMnO_3$ and (b) $LaMnO_3$ at room temperature.

Figure 1 shows the reflectivity spectra of $CaMnO_3$ and $LaMnO_3$. The phonon structures below 100 meV are not plotted, since we are interested only in the optical excitations of electronic origins. In order to obtain an optical conductivity spectrum, $\sigma(\omega)$, of each sample, the Kramers-Kronig transformation was used. For this analysis, reflectivity below 5 meV was extrapolated to be constant. For a high-frequency region, reflectivity at 30 eV was extended up to 40 eV, above which ω^{-4} dependence was assumed. The experimental spectra of $\sigma(\omega)$ above 100 meV are shown in Fig. 2. For $CaMnO_3$, there are four apparent peaks, denoted by α, β, γ, and δ, in the energy range up to 30 eV. For $LaMnO_3$, there are five apparent peaks, denoted by A, B, C, D, and E.

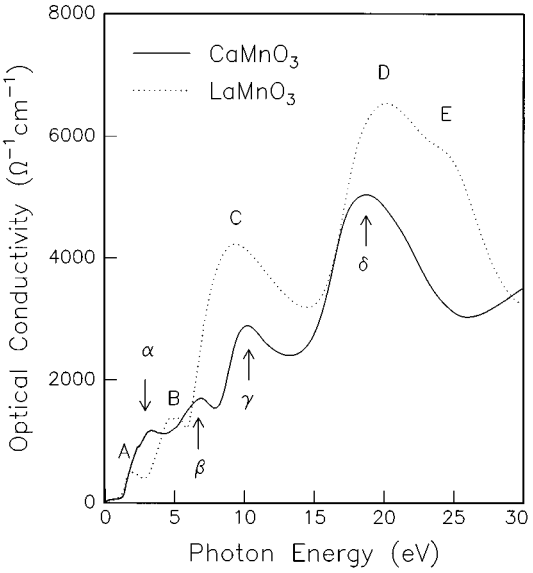

FIG. 2. Optical conductivity spectra of $CaMnO_3$ and $LaMnO_3$. Labeled greek and latin letters represent apparent peaks in the spectra.

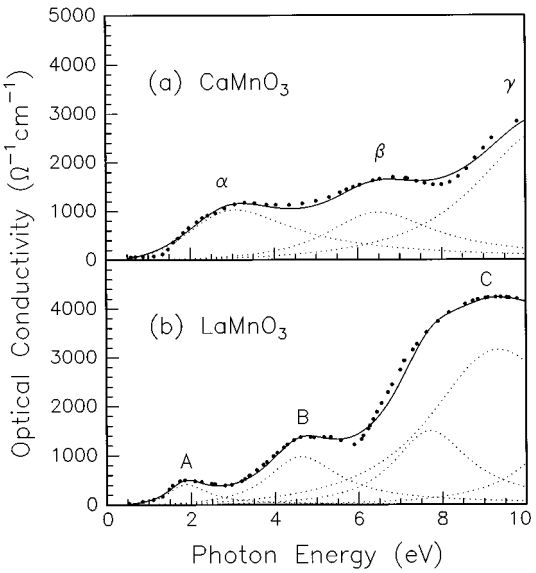

FIG. 3. Detailed optical conductivity spectra, below 10 eV, of (a) $CaMnO_3$ and (b) $LaMnO_3$. The solid circles and lines represent the experimental data and the fitting results, respectively. The dotted lines show contributions of each Lorentz oscillator.

To get a better understanding on the electronic structure near E_F, we fitted the conductivity data up to 10 eV with a series of the Lorentz oscillator functions:

$$\sigma(\omega)=\sum_i \frac{S_i\Gamma_i\omega^2}{(\omega^2-\omega_i^2)^2+\Gamma_i^2\omega^2}, \tag{1}$$

where S_i, ω_i, and Γ_i represent the strength, the frequency, and the damping constant of the ith Lorentz oscillator, respectively.[14] As shown in Fig. 3(a), $\sigma(\omega)$ of $CaMnO_3$ below 10 eV can be represented by three Lorentz oscillators, each of whose contribution is shown as a dotted line. The first two oscillators, corresponding to α and β, are located around 3.1 and 6.5 eV, respectively, with similar strengths and widths. The third one, corresponding to γ, has larger strength and width. Figure 3(b) shows a detailed $\sigma(\omega)$ spectrum for $LaMnO_3$. The first two oscillators, corresponding to A and B, are located around 1.9 and 4.6 eV, respectively. It was found that the peak C should be represented by at least three oscillators. A summary of the values of the fitting parameters is given in Table I.

From the Fermi ''golden rule,''[14] an optical transition rate, which is proportional to the strength of a Lorentz oscillator, from an initial state $|i\rangle$ to a final state $|f\rangle$ can be written as

$$I_{i\to f}\sim|\langle f|M|i\rangle|^2\rho_f\rho_i, \tag{2}$$

where ρ_i and ρ_f are densities of states for $|i\rangle$ and $|f\rangle$, respectively. In the manganese oxides, the Mn e_g and the Mn t_{2g} orbitals form σ and π bondings with the O $2p$ orbitals, respectively. Overlap of the corresponding wave function with the O $2p$ orbitals should be much smaller for t_{2g}. So, the optical transitions between O $2p$ and t_{2g} levels were assumed to be negligible in the $\sigma(\omega)$ spectra in Fig. 3.

TABLE I. Values of Lorentz oscillator fitting parameters for $CaMnO_3$ and $LaMnO_3$. All frequencies and damping constants are in units of eV.

Oscillator	S_i	ω_i	Γ_i	Assignment
		$CaMnO_3$		
α $(i=1)$	3210	3.07	3.12	O $2p \rightarrow e_{g\uparrow}$
β $(i=2)$	3080	6.49	3.16	O $2p \rightarrow e_{g\downarrow}$
γ $(i=3)$	11200	10.5	4.24	O $2p \rightarrow$ Ca $3d$
		$LaMnO_3$		
A $(i=1)$	470	1.89	1.13	$e^1_{g\uparrow} \rightarrow e^2_{g\uparrow}$
B $(i=2)$	2030	4.63	2.08	O $2p \rightarrow e^2_{g\uparrow}$
C $(i=3)$	3290	7.71	2.20	O $2p \rightarrow e_{g\downarrow}$
C $(i=4)$	13200	9.35	4.18	O $2p \rightarrow$ La $5d$
C $(i=5)$	3870	11.1	2.49	$e^1_{g\uparrow} \rightarrow$ Mn $4s/4p$

First, let us consider the $\sigma(\omega)$ spectrum of $CaMnO_3$, which is shown in Fig. 3(a). The first and the second Lorentz oscillators are assigned to O $2p \rightarrow e_{g\uparrow}$ and O $2p \rightarrow e_{g\downarrow}$ transitions, respectively. The $e_{g\downarrow}$ band should be higher in energy than the $e_{g\uparrow}$ band due to the Hund coupling with the $t_{2g\uparrow}$ core spins. And the third oscillator is assigned mainly to O $2p \rightarrow$ Ca $3d$ transition. These $p \rightarrow d$ transitions are dipole allowed and have charge-transfer characteristics in nature. Since the first two transitions have the same initial state and similar final states, they should have similar strengths and widths. As shown in Table I, the first and second oscillators have similar values of S_i and Γ_i. It also can be seen that the value of Γ_3 is larger than that of Γ_1 or Γ_2. This fact is in good agreement with the XAS result that the Ca $3d$ band is more widely spread in energy than any Mn $3d$ band.[5]

Second, let us turn to the $\sigma(\omega)$ spectrum of $LaMnO_3$, shown in Fig. 3(b). Here, the $e_{g\uparrow}$ band splits into two, $e^1_{g\uparrow}$ and $e^2_{g\uparrow}$ bands. The $e^1_{g\uparrow}$ band should be overlapped with the O $2p$ band due to strong hybridization, while the $e^2_{g\uparrow}$ band forms the lowest-lying empty conduction band. Since S_2 and S_3 of this compound are quite comparable to S_1 and S_2 of $CaMnO_3$ within a factor of 2, the second and the third oscillators are assigned to O $2p \rightarrow e^2_{g\uparrow}$ and O $2p \rightarrow e_{g\downarrow}$ transitions, respectively. The former has smaller strength than the latter, because the density of states of the $e^2_{g\uparrow}$ band is about half that of the $e_{g\downarrow}$ band. The fourth and the fifth are attributed to O $2p \rightarrow$ La $5d$, and Mn $e^1_{g\uparrow} \rightarrow$ Mn $4s/4p$, respectively. Mn $4s$ and $4p$ bands are considered to be significantly delocalized, forming an overlapping Mn $4s/4p$ band.[4]

Note that, for $LaMnO_3$, S_1 is smaller than S_2 or S_3 by an order of magnitude, suggesting that the character of the first transition might be different. The first Lorentz oscillator is assigned to the $e^1_{g\uparrow} \rightarrow e^2_{g\uparrow}$ transition. If it is a $d \rightarrow d$ transition between unhybridized d bands, it should be dipole forbidden, so its strength is expected to be orders of magnitude smaller than the second one. However, the relatively large overlap of the O $2p$ and the Mn e_g wave functions will hybridize these bands. (Indeed, hybridization between O $2p$ and metal $3d$ wave functions is a common feature in ABO_3-type transition-metal oxides.[15]) In $LaMnO_3$, many spectroscopic studies have confirmed that the band mixing is quite strong and the $e^1_{g\uparrow}$ band contains O $2p$ as well as Mn $3d$ characters.[7] Therefore, the first oscillator will include the contribution of O $2p \rightarrow e^2_{g\uparrow}$ dipole transition also.

Based on the above analyses, we modeled band diagrams for $CaMnO_3$ and $LaMnO_3$. The schematic band diagrams, determined from our optical spectra in conjunction with other spectroscopic data, are shown in Figs. 4(a) and 4(b).

The double peaks, which were observed around -7 and -3 eV in $CaMnO_3$,[5] are identified as Mn $t_{2g\uparrow}$ and O $2p$ bands, respectively. If their positions are reversed, some discrepancies occur. Assume that the $t_{2g\uparrow}$ band is closer to E_F than the O $2p$ band. Then, the first and the second oscillators in Fig. 3(a) should come from the $t_{2g\uparrow}$ band, since any transition originating from the O $2p$ band to a conduction band will make ω_i $(i=1$ or $2)$ larger than 7 eV. However, there exists only one transition allowed by the spin selection rule: i.e., $t_{2g\uparrow} \rightarrow e_{g\uparrow}$. This is in contradiction with the experimental fact that two Lorentz oscillators exist below 7 eV.

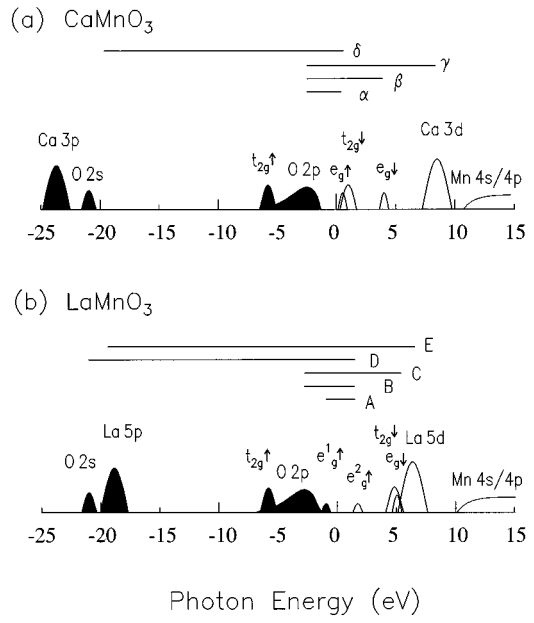

FIG. 4. Schematic band diagrams of (a) $CaMnO_3$ and (b) $LaMnO_3$. The solid and the open areas represent valence and conduction bands, respectively. The Mn e_g and the Mn t_{2g} bands are abbreviated as e_g and t_{2g}, respectively.

One may argue that there might be some excitonic effects that will make ω_i smaller by 1 or 2 eV than the difference between the initial and the final energies. Even with such effects, the $t_{2g\uparrow} \rightarrow e_{g\uparrow}$ transition should correspond to the first oscillator, if the $t_{2g\uparrow}$ band is located closer to E_F. Then, the second oscillator should originate from the O $2p \rightarrow e_{g\uparrow}$ transition. It is a dipole-allowed transition, which should have a much stronger strength than the first oscillator corresponding to a $d \rightarrow d$ transition. However, our experimental data show that S_1 is very close to S_2 of $CaMnO_3$. Therefore, it is concluded that *the Mn $t_{2g\uparrow}$ band is located at a lower energy than the O 2p band.*

With the identification of the valence bands near E_F, the schematic diagram for $CaMnO_3$ can be drawn. As shown in Fig. 4(a), positions of $e_{g\uparrow}$, $e_{g\downarrow}$, and Ca $3d$ bands can be marked as the final states of α, β, and γ transitions using the ω_i values in Table I. Other valence bands, such as Ca $3p$ and O $2s$, are positioned according to XPS data.[5] And, some conduction bands, such as $t_{2g\downarrow}$ and Mn $4s/4p$ bands, are positioned according to O $1s$ XAS data.[5] Then, the diagram becomes consistent with the optical spectrum shown in Fig. 3(a). The O $2p \rightarrow$ Mn $4s/4p$ and $t_{2g\uparrow} \rightarrow$ Mn $4s/4p$ transitions form a broad background in the excitations above 15 eV. In addition, the small peak δ might be originated from O $2s \rightarrow$ Mn $3d$ transition, which was similarly identified in $LaVO_3$.[16]

In $LaMnO_3$, the relative position between the $t_{2g\uparrow}$ and O $2p$ bands should be the same as that in $CaMnO_3$. If not, S_2 of $LaMnO_3$ should be much smaller than S_1 of $CaMnO_3$. For $LaMnO_3$, the $e^1_{g\uparrow}$ band is located closer to E_F than the other bands, contrary to the band calculation results of Satpathy, Popović, and Vukajlović.[9] From UPS measurements, Saitoh *et al.*[6] suggested that the $e^1_{g\uparrow}$ band should exist close to E_F, however, the existence of the $e^1_{g\uparrow}$ band was not clear since it was located at the rising edge of the O $2p$ band. Our optical data indicate the existence of the $e^1_{g\uparrow}$ band near E_F more clearly.

The schematic diagram for $LaMnO_3$ can be also drawn. As shown in Fig. 4(b), positions of $e^2_{g\uparrow}$, $e_{g\downarrow}$, and La $5d$ bands can be determined from the optical transitions, A, B, and C. The other valence bands and conduction bands are positioned according to XPS data[5,6] and O $1s$ XAS data,[4–6] respectively. Then, the peaks D and E correspond to O $2s \rightarrow e^2_{g\uparrow}$ and La $5p \rightarrow$ La $5d$ transitions, respectively.

The double exchange (DE) mechanism based on the large Hund coupling between e_g and t_{2g} electrons has been traditionally used to explain the coexistence of ferromagnetic ordering and metallic phase in $La_{1-x}Ca_xMnO_3$. However, recent works by Millis, Littlewood, and Shraiman[17] suggested that the effect due to the DE alone is not large enough to explain the CMR. They proposed that a dynamic JT splitting should be included. From the band diagrams in Fig. 4, we tried to extract values of the t_{2g}-e_g Hund exchange and the JT stabilization energies.

In $CaMnO_3$, where the $t_{2g\uparrow}$ levels are filled, the energy difference between the $e_{g\uparrow}$ and the $e_{g\downarrow}$ bands, both unfilled, corresponds to the t_{2g}-e_g Hund exchange energy. In Table I, it is found to be 3.4 eV as determined by the energy difference of the second and first oscillators. This value is similar to the values of the Mn d-band exchange splitting, i.e., $\sim$3.0 eV for $CaMnO_3$ and $\sim$3.5 eV for $LaMnO_3$, calculated by the local spin-density approximation.[10] However, it is larger than the t_{2g} exchange value of $\sim$1.5 eV for $LaMnO_3$, calculated by the local-density approximation plus on-site Coulomb interaction.[11] It is also larger than the on-site exchange energy of $\sim$2.0 eV for $La_{0.825}Sr_{0.175}MnO_3$, estimated from its temperature-dependent spectral weight changes.[3]

In $LaMnO_3$, the energy separation of $E(e^2_{g\uparrow})$-$E(e^1_{g\uparrow})$, i.e., about 1.9 eV, can result from the JT splitting and on-site Coulomb interaction. The Coulomb interaction will be effective only for the $e^1_{g\uparrow}$ electrons and move the corresponding level to a lower energy.[11] Neglecting such a correlation effect, $E(e^2_{g\uparrow})$-$E(e^1_{g\uparrow})$ corresponds to the energy separation of the JT split bands, $4E_0$, where E_0 is the JT energy gain in forming a local lattice distortion.[18] So, E_0 should have an upper bound of about 0.5 eV, in good agreement with the proposed value by Millis, Littlewood, and Shraiman.[17] There are some experimental works that indicate that a polaron plays an important role in $La_{1-x}Ca_xMnO_3$.[12] However, more investigations are required to decide whether the polaron due to the dynamic JT splitting is essential to explain the CMR.

In summary, we have investigated the electronic band structures of $CaMnO_3$ and $LaMnO_3$ near E_F, using quantitative analyses of optical conductivity spectra. It was found that the O $2p$ band is located closer to E_F than the Mn $t_{2g\uparrow}$ band. For $LaMnO_3$, the $e^1_{g\uparrow}$ band is located very close to E_F.

We would like to acknowledge the financial support by Seoul National University Dae Woo Research Fund, by the Ministry of Education through the Inter-University Center for Natural Science Research Facilities (BSRI-96-7402), and by the Korea Science and Engineering Foundation through Grant No. 96-0702-02-01-3. Experiments at PLS were supported in part by MOST and POSCO.

*Electronic address: hoon@phya.snu.ac.kr
†Electronic address : twnoh@phya.snu.ac.kr

[1] S. Jin *et al.*, Science **264**, 413 (1994); P. Schiffer, A. P. Ramirez, W. Bao, and S.-W. Cheong, Phys. Rev. Lett. **75**, 3336 (1995).
[2] G. H. Jonker and J. H. van Santen, Physica **16**, 337 (1950).
[3] Y. Okimoto *et al.*, Phys. Rev. Lett. **75**, 109 (1995).
[4] M. Abbate *et al.*, Phys. Rev. B **46**, 4511 (1992).
[5] J. -H. Park *et al.*, Phys. Rev. Lett. **76**, 4215 (1996).
[6] T. Saitoh *et al.*, Phys. Rev. B **51**, 13 942 (1995).
[7] A. Chainani, M. Mathew, and D. D. Sarma, Phys. Rev. B **47**, 15 397 (1993).
[8] D. D. Sarma *et al.*, Phys. Rev. Lett. **75**, 1126 (1995).
[9] S. Satpathy, Z. S. Popović, and F. R. Vukajlović, Phys. Rev. Lett. **76**, 960 (1996).
[10] W. E. Pickett and D. J. Singh, Phys. Rev. B **53**, 1146 (1996).
[11] I. Solovyev, N. Hamada, and K. Terakura, Phys. Rev. B **53**, 7158 (1996).
[12] K. H. Kim *et al.*, Phys. Rev. Lett. **77**, 1877 (1996).

[13] K. H. Kim *et al.*, Phys. Rev. B **55**, 4023 (1997).
[14] F. Wooten, *Optical Properties of Solids* (Academic Press, New York, 1972).
[15] A. Fujimori and Y. Tokura, *Spectroscopy of Mott Insulators and Correlated Metals* (Springer-Verlag, Berlin, 1995).
[16] T. Arima and Y. Tokura, J. Phys. Soc. Jpn. **64**, 2488 (1995).
[17] A. J. Millis, P. B. Littlewood, and B. I. Shraiman, Phys. Rev. Lett. **74**, 5144 (1995).
[18] M. D. Kaplan and B. G. Vekhter, *Cooperative Phenomena in Jahn-Teller Crystals* (Plenum, New York, 1995).